PCCP

ROYAL SOCIETY OF CHEMISTRY

PAPER

View Article Online
View Journal | View Issue

Cite this: *Phys. Chem. Chem. Phys.*, 2024, **26**, 11988

Counterion effects on the mesomorphic and electrochemical properties of guanidinium salts†

Max Ebert, ‡[a] Alyna Lange,‡[b] Michael Müller,‡[a] Eugen Wuckert,[a] Frank Gießelmann, [c] Tillmann Klamroth, [b] Anna Zens,[a] Andreas Taubert *[b] and Sabine Laschat *[a]

Received 25th January 2024,
Accepted 13th March 2024

DOI: 10.1039/d4cp00356j

rsc.li/pccp

Ionic liquid crystals (ILCs) combine the ion mobility of ionic liquids with the order and self-assembly of thermotropic mesophases. To understand the role of the anion in ILCs, wedge-shaped arylguanidinium salts with tetradecyloxy side chains were chosen as benchmark systems and their liquid crystalline self-assembly in the bulk phase as well as their electrochemical behavior in solution were studied depending on the anion. Differential scanning calorimetry (DSC), polarizing optical microscopy (POM) and X-ray diffraction (WAXS, SAXS) experiments revealed that for spherical anions, the phase width of the hexagonal columnar mesophase increased with the anion size, while for non-spherical anions, the trends were less clear cut. Depending on the anion, the ILCs showed different stability towards electrochemical oxidation and reduction with the most stable being the PF_6 based compound. Cyclic voltammetry (CV) and density functional theory (DFT) calculations suggest a possible contribution of the guanidinium cation to the oxidation processes.

Introduction

Among the large class of thermotropic liquid crystals, which form bulk mesophases (*i.e.* liquid crystalline phases) of orientationally ordered lamellar, columnar or cubic geometries upon change of the temperature, ionic liquid crystals (ILCs) constitute an important subclass.[1–10] From a molecular perspective, ILCs carry cationic (or less often anionic) headgroups, nonpolar side chains with or without mesogenic subunits and inorganic (or organic) counter ions, resulting in strong Coulomb interaction and nano segregation into mesophases showing anisotropic physical properties on the one hand and on the other hand, ionic liquids (ILs) are organic, low melting salts, often with adjustable polarity, fluidity, viscosity and a wide electrochemical window.[1–10] These unique properties make ILCs promising candidates for a variety of applications, in particular as electrolytes in dye sensitized solar cells (DSSCs),[11–14] batteries, fuel cells and capacitor materials.[15–17] Despite the growing interest in electrochemical applications, most electric and ionic conductivity as well as cyclic voltammetry studies have been carried out with imidazolium ILCs.[1] Guanidinium ILCs, on the other hand, provide various opportunities to tailor their liquid crystalline self-assembly regarding mesophase geometry and temperature range[18–23] to obtain rare mesophases such as tilted lamellar smectic C phase (SmC)[24,25] and de Vries (*i.e.* minimal layer contraction at the transition from tilted SmC to non-tilted SmA phase),[24,25] or photoresponsive behavior.[26] ILs based on guanidinium cations and trifluorosulfonimide anions have been previously investigated regarding their electrochemical properties[27–29] as additives in electrolytes for DSSCs,[30] as well as guanidinium-functionalized anion exchange polymer electrolytes.[31] In addition, the electrochemical properties of guanidines and the respective guanidinium salts were studied with respect to their applications as redox active ligands of metal complexes.[32–35] Moreover, aminocyclopropenium ions have been introduced as deltic guanidinium ions, *i.e.* macrosteres of the guanidinium ions,[36,37] which were successfully employed as redox-active organic salt for Na-ion batteries,[38] persistent radical cations,[39] polyelectrolytes,[40] polymerized ionic liquids for ion transport[41] and materials for electrophotocatalysis.[42] ILCs are expected to have certain advantages over ILs in battery and solar cell applications, such as 1D, 2D or 3D ordered charge transport depending on the mesophase type.[43,44] Thus, a basic understanding of both mesomorphic properties, *e.g.* phase transition temperatures and phase width as well as geometry and packing behavior of the liquid crystalline self-assembly and electrochemical

[a] *Institut für Organische Chemie, Universität Stuttgart, Pfaffenwaldring 55, Stuttgart 70569, Germany. E-mail: sabine.laschat@oc.uni-stuttgart.de*
[b] *Institut für Chemie, Universität Potsdam, Institut für Chemie, Karl-Liebknecht-Str. 24-25, Golm 14476, Germany. E-mail: ataubert@uni-potsdam.de*
[c] *Institut für Physikalische Chemie, Universität Stuttgart, Pfaffenwaldring 55, Stuttgart 70569, Germany. E-mail: f.giesselmann@ipc.uni-stuttgart.de*

† Electronic supplementary information (ESI) available. See DOI: https://doi.org/10.1039/d4cp00356j

‡ These coauthors contributed equally to this work.

properties of the respective ILCs is required, as the electrochemical stability towards oxidation and reduction directly influences the useable electrochemical window in an application.[45,46] Indeed, many ILs and ILCs have been investigated for their electrochemical stability windows.[47–53] However, electrochemical studies of guanidinium-based compounds are quite rare and there are no reports on the electrochemical properties of guanidinium-based ILCs.[27,29,54–63]

On the other hand, counterions also play an important role in both the mesomorphic and electrochemical properties[1,2,53,65–71] of ILCs as well as hydrophilicity, viscosity, and electrochemical window.[27,72–74]

Thus, in order to understand their liquid crystalline self-assembly in the bulk phase and their electrochemical behavior in solution, we investigated a series of wedge-shaped 3,4,5-trisalkoxy-phenyl-guanidinium salts **Gua(14)X** with different counterions X = Cl, Br, I, BF_4, PF_6, OMs, SCN, $N(CN)_2$, NO_3, NTf_2, OTf, OTs, N_3, CN, OCN, OAc. The 3,4,5-trisalkoxy-phenyl-guanidinium mesogen **Gua(14)** was chosen as a cationic moiety because it is a very robust mesogen, forming a columnar mesophase in the presence of the chloride anion and undulated lamellar SmA phases for bulky divalent Mo cluster anions[64] (Fig. 1). Our current study revealed that the electrochemical stability window of these guanidinium ILCs in solution was strongly affected by the counterion. In the bulk mesophase, the counterion had a pronounced influence on the stability and temperature range, whereas the packing geometry was little affected. The details are discussed below.

Results and discussion

Synthesis and NMR studies of guanidinium ILCs

The guanidinium salts **Gua(14)X** were prepared *via* salt metathesis from the known tristetradecyloxyphenylguanidinium chloride **Gua(14)Cl**[64] according to the procedure proposed by Butschies[18] (Scheme 1). After recrystallization, the resulting guanidinium salts **Gua(14)X** were isolated in 79–91% yield.

Upon exchange of the anion, a characteristic upfield shift of the guanidinium N–H signal was observed, as exemplified for **Gua(14)Br** (Fig. 2b) and **Gua(14)N(CN)$_2$** (Fig. 2c) as compared to **Gua(14)Cl** (Fig. 2a). A stacked plot showing the NMR spectra of the whole series **Gua(14)X** is shown in Fig. S1 (ESI†). The chemical shift δ(N–H) decreased with increasing anion size (Fig. S2, ESI†). These observations are in good agreement with previously reported NMR studies of guanidinium ILCs.[18,75] We surmised that the observed counterion dependent chemical shift of the N–H signal in the ^{1}H NMR spectrum might be caused by ion pairing in solution, as was independently reported by Aidas[76] for imidazolium and by Saielli[77] for pyridinium ionic liquids. Our concentration-dependent NMR studies of **Gua(14)Cl** in $CDCl_3$ revealed that the guanidinium N–H signal shifted only very little with decreasing concentration. In addition, a broadening and doubling of the N–H peak were observed (Fig. S3, ESI†). These results suggest that the ion pairs in **Gua(14)X** are generated by a combination of Coulomb interaction and H-bonding,[78,79] while the peak broadening is probably due to the formation of H-bonded aggregates resulting in rotameric equilibria (for a detailed analysis of such

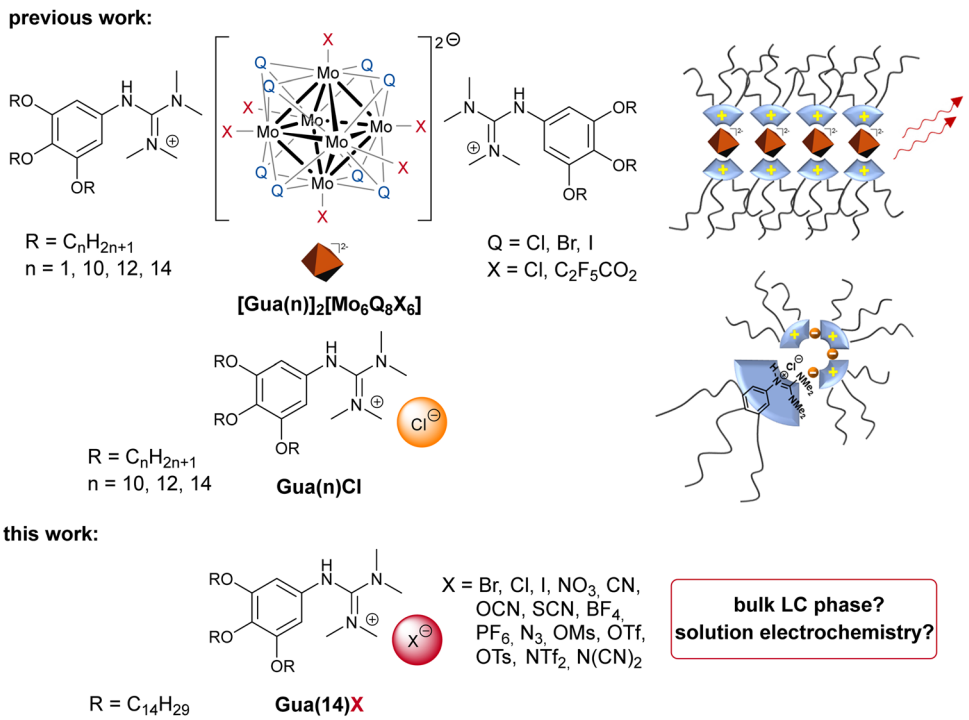

Fig. 1 Preliminary work on luminescent clustomesogens **[Gua(n)]$_2$[Mo$_6$Q$_8$X$_6$]**[64] derived from guanidinium ILCs **Gua(n)Cl** and our new studies on one of these ILCs (**Gua(14)X**) with different anions X.

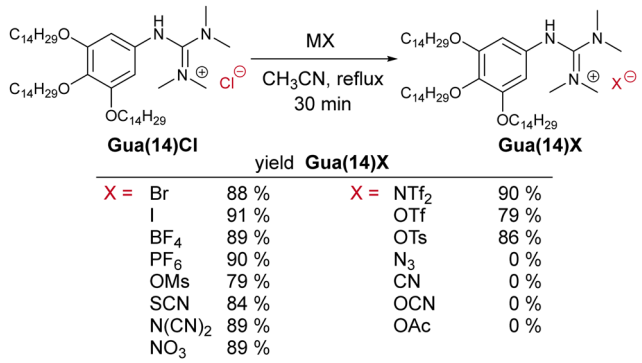

yield **Gua(14)X**

X =			X =	
	Br	88 %	NTf_2	90 %
	I	91 %	OTf	79 %
	BF_4	89 %	OTs	86 %
	PF_6	90 %	N_3	0 %
	OMs	79 %	CN	0 %
	SCN	84 %	OCN	0 %
	$N(CN)_2$	89 %	OAc	0 %
	NO_3	89 %		

Scheme 1 Synthesis of **Gua(14)X**.

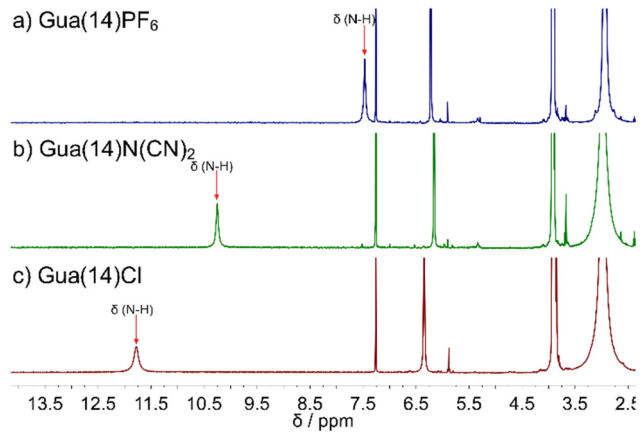

Fig. 2 Sections of the ^{1}H NMR spectra (400 MHz, r.t., $CDCl_3$) of guanidinium salts (a) **Gua(14)PF_6** (blue), (b) **Gua(14)$N(CN)_2$** (green) and (c) **Gua(14)Cl** (red) showing the anion-dependent shift of the guanidinium N–H signal.

guanidinium rotamers, see ref. 18 and 75). The importance of H-bonding between the anion and cation was also pointed out by Donnio for azatriphenylene ILCs.[70] In addition, we performed NMR experiments in different solvents, which revealed that the δ(N–H) shift decreased with increasing polarity of solvents (Fig. S4, ESI†), presumably due to the weakening of the contact ion pairs and formation of solvent-separated ion pairs.

It should be noted that any attempts to prepare guanidinium ILCs **Gua(14)X** with counterions of weak acids, *i.e.* X = N_3, OAc, CN, OCN failed (Scheme 1). The resulting reaction products from the salt metathesis did not show the characteristic HN=C signal for the guanidinium moiety in the ^{1}H NMR spectra (for details, see Fig. S1, ESI†). Presumably, for guanidinium salts with anions of weak acids, the acid–base equilibrium is shifted towards the neutral guanidine base and HX.[80] Indeed, the free guanidine **Gua(14)** could be isolated and characterized by NMR (for details, see ESI†).[81] In the bulk phase, such equilibration would lead to evaporation of the acids HN_3, HOAc, HCN, and HOCN during repetitive heating/cooling cycles in DSC, POM or XRD analyses. Thus, further experiments with these counterions were abandoned.

Mesomorphic properties of guanidinium ILCs

Investigation by differential scanning calorimetry (DSC) and polarizing optical microscopy (POM) revealed enantiotropic mesomorphism for guanidinium salts **Gua(14)X** with counterions X = Cl, Br, I, BF_4, PF_6, OMs, SCN, $N(CN)_2$, NO_3, while guanidinium salts with X = NTf_2, OTf, OTs were non-mesomorphic (Table 1) (all DSC curves are shown in Fig. S7 and S8, ESI†).

The data in Fig. 3 suggest that there are four types of guanidinium salts **Gua(14)X** depending on the size and topology of the anion. For example, guanidinium salts with spherical anions X = Cl, Br, I, BF_4, PF_6 exhibited broad mesophases with up to 84 K phase widths and clearing temperatures up to 112 °C. The anion size had only little effect on the phase behavior. For example, although the anion diameter of PF_6 is

Table 1 Phase transition temperatures T in °C (−enthalpies ΔH in kJ mol^{-1}, if available) of guanidinium ILCs **Gua(14)X**[ab]

X	Cr_3			Cr_2			Cr_1			Col_h			I	
Cl	—			—			●	34.44	(−34.74)	●	86.96	(−55.09)	●	2nd H
	—			—			●	25.19	(32.09)	●	89.28	(1.18)	●	2nd C
Br	—			●	34.44	(−31.94)	●	85.63	(−0.45)	●	93.11	(−1.03)	●	2nd H
	—			—			●	25.22	(31.84)	●	91.43	(1.09)	●	2nd C
I	—			—			●	33.89	(−33.90)	●	100.37	(−0.99)	●	2nd H
	—			—			●	24.79	(32.86)	●	99.12	(0.99)	●	2nd C
BF_4	—			—			●	36.16	(−33.8)	●	112.30	(−1.0)	●	2nd H
	—			—			●	27.85	(31.5)	●	112.04	(1.1)	●	2nd C
PF_6	—			●	34.16	(−32.96)	●	42.82	(−9.89)	●	106.18	(−1.02)	●	2nd H
	—			—			●	25.76	(33.80)	●	105.92	(1.03)	●	2nd C
OMs	—			—			●	35.01	(−37.15)	●	82.30	(−1.06)	●	2nd H
	—			—			●	25.62	(35.3)	●	82.60	(1.02)	●	2nd C
SCN	●	35.40	(−10.63)	●	38.02	(−16.37)	●	55.00	(−54.73)	●	76.59	(−0.85)	●	2nd H
	—			—			●	30.15	(40.0)	●	75.02	(0.84)	●	2nd C
$N(CN)_2$	—			—			●	45.24	(−27.11)	●	70.59	(−22.87)	●	2nd H
	—			—			●	40.14	(51.61)	●	70.33	(0.84)	●	2nd C
NO_3	●	11.13	(−10.47)	●	33.94	(−1.80)	●	57.17	(−12.03)	●	104.13	(−1.11)	●	2nd H
	●	19.91	(8.61)	●	29.13	(1.94)	●	46.29	(11.95)	●	103.98	(1.02)	●	2nd C

[a] Values were obtained from DSC with cooling/heating rates of 5 K min^{-1}. [b] The following phases were observed: Cr_1, Cr_2, Cr_3 crystalline, Col_h hexagonal columnar, I isotropic. ● phase observed,—phase not observed.

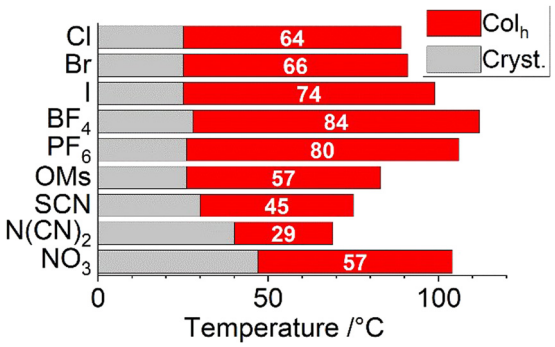

Fig. 3 Mesophase widths [K] of guanidinium ILCs **Gua(14)X** with different anions.

1.5 times larger than Br, both guanidinium salts **Gua(14)Br** and **Gua(14)PF$_6$** showed similar melting and clearing transition. The second type of guanidinium salts **Gua(14)X** carrying anions derived from Brønsted acid sulfonates were mostly non-mesomorphic (X = OTf, OTs) except for the mesylate (X = OMs), which displayed a broad mesophase between 26 °C and 83 °C. The third type contained linear anions, such as X = SCN, OCN, N_3. But only the synthesis of **Gua(14)SCN** led to the desired product, and it exhibited mesomorphic properties.

The fourth type consisted of bent or C_3-symmetrical anions such as N(CN)$_2$ or NO_3. Both guanidinium salts **Gua(14)N(CN)$_2$** and **Gua(14)NO$_3$** displayed mesophases, however the temperature range for nitrate was larger as compared to dicyanamide, presumably due to the improved delocalization and net charge compensation in the latter case. The following phases were observed: hexagonal columnar Col$_h$, crystalline Cryst. Assignment of phase types was based on the XRD experiments. For details, see Fig. 5 and Table 2 and the corresponding text.

Under the POM, all mesomorphic guanidinium salts displayed fan-shaped textures, indicating the presence of a columnar mesophase in analogy to the known chloride salt

Table 2 XRD results of guanidinium ILCs **Gua(14)X**[ab]

Gua(14)X	Anion X (θ/Å)	Mesophase (T/°C)	Reflexes/Å exp. (calc.)	Miller indices	Lattice parameters/Å
Gua(14)Cl	Cl 3.62	Col$_h$ at 65 °C *P6mm*	33.24 19.20 (19.19) 16.62 (16.62) 4.65	(10) (11) (20) Halo	a = 38.38
Gua(14)Br	Br 3.92	Col$_h$ at 65 °C *P6mm*	33.23 19.18 (19.19) 16.60 (16.62) 4.56	(10) (11) (20) Halo	a = 38.38
Gua(14)I	I 4.40	Col$_h$ at 65 °C *P6mm*	29.86 4.52	(10) Halo	a = 34.48
Gua(14)BF4	BF$_4$ 4.64	Col$_h$ at 65 °C *P6mm*	34.06 19.77 (19.67) 17.07 (17.03) 4.12	(10) (11) (20) Halo	a = 39.33
Gua(14)PF$_6$	PF$_6$ 5.80	Col$_h$ at 65 °C *P6mm*	33.18 19.16 (19.67) 16.60 (17.03) 4.59	(10) (11) (20) Halo	a = 38.32
Gua(14)OMs	Oms 3.77	Col$_h$ at 65 °C *P6mm*	33.85 19.52 (19.54) 16.93 (16.93) 4.53	(10) (11) (20) Halo	a = 39.09
Gua(14)SCN	SCN 4.26	Col$_h$ at 65 °C *P6mm*	32.88 18.96 (18.98) 16.47 (16.44) 4.53	(10) (11) (20) Halo	a = 37.97
Gua(14)N(CN)$_2$	N(NC)$_2$ 4.51	Col$_h$ at 65 °C *P6mm*	34.77 20.08 (20.07) 17.39 (17.38) 4.52	(10) (11) (20) Halo	a = 40.15
Gua(14)NO$_3$	NO$_3$ 4.00	Col$_h$ at 65 °C *P6mm*	34.01 19.70 (19.64) 17.01 (17.01) 4.59	(10) (11) (20) Halo	a = 39.27

[a] Anion diameters (except OMs, N(CN)$_2$) were taken from ref. 84. [b] Anion diameters of mesylate and dicyanamide were estimated from Chem3D ball & stick models.

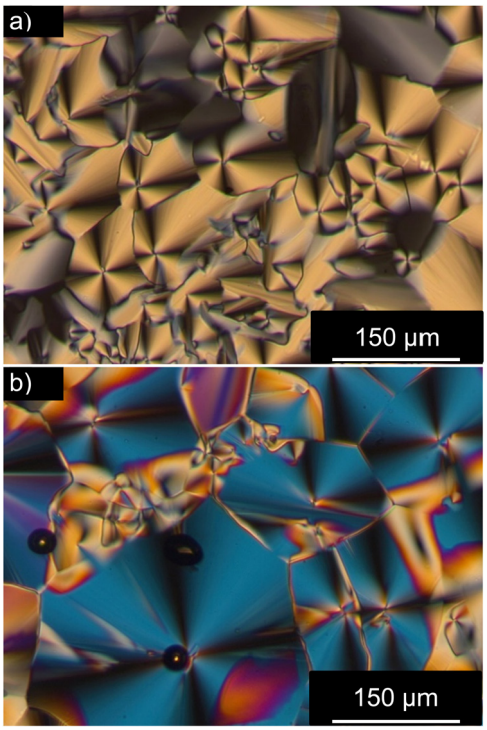

Fig. 4 POM textures of (a) **Gua(14)Br** at 98 °C and (b) **Gua(14)N(CN)$_2$** at 71 °C upon cooling from the isotropic phase (100× magnification, heating/cooling rate 5 K min^{-1}).

Gua(14)Cl.[64] Typical examples are shown in Fig. 4 for the bromides, **Gua(14)Br** (Fig. 4a) and dicyanamide **Gua(14)N(CN)$_2$** (Fig. 4b). The POM textures of all guanidinium salts are summarized in Fig. S5 and S6 (ESI†).

The mesophase geometry of the liquid crystalline guanidinium salts **Gua(14)X** was assigned by X-ray diffraction (XRD) using small- and wide-angle scattering (SAXS, WAXS), respectively. For example, bromide **Gua(14)Br** showed three sharp reflections at 33.24 Å, 19.20 Å and 16.62 Å respectively, which were assigned to the (10) (11) and (20) reflections with reciprocal *d*-spacings of $1:1/\sqrt{3}:1/2$ of a hexagonal columnar (Col_h) mesophase with space *P6mm* and a lattice parameter a = 38.38 Å (Fig. 5a). In the wide-angle section, a broad halo around 4.6 Å was visible due to the liquid-like disorder of the alkyl side chains (Fig. 5b).

In agreement with the DSC results, **Gua(14)PF$_6$** exhibited a similar diffractogram and lattice parameter (a = 38.32 Å) (Fig. 5c and d) despite a much larger size of the PF_6 anion. Overall, when comparing the lattice parameters of the various guanidinium salts **Gua(14)X** shown in Table 2, no obvious trends were visible. This is quite surprising, as one would expect that the counterion contributes to a significant extent to the size of the pizza-slice packing (Fig. 6), which we propose for these wedge-shaped ILCs in agreement with the previous work.[64,69,75,82,83] Details of the XRD data are summarized in Fig. S9–S11 (ESI†). It should be noted that in several reported cases, anion variation does not change the mesophase geometry or space group, *i.e.* for wedge-shaped mesogens with 3 alkoxy side chains, the space filling of the cation strongly favors the hexagonal columnar (*P6mm*) geometry.[69,75,83] However, for ILCs with bulky or non-spherical anions (*e.g.* with long side chains), mesophases with other space groups can be formed.[70]

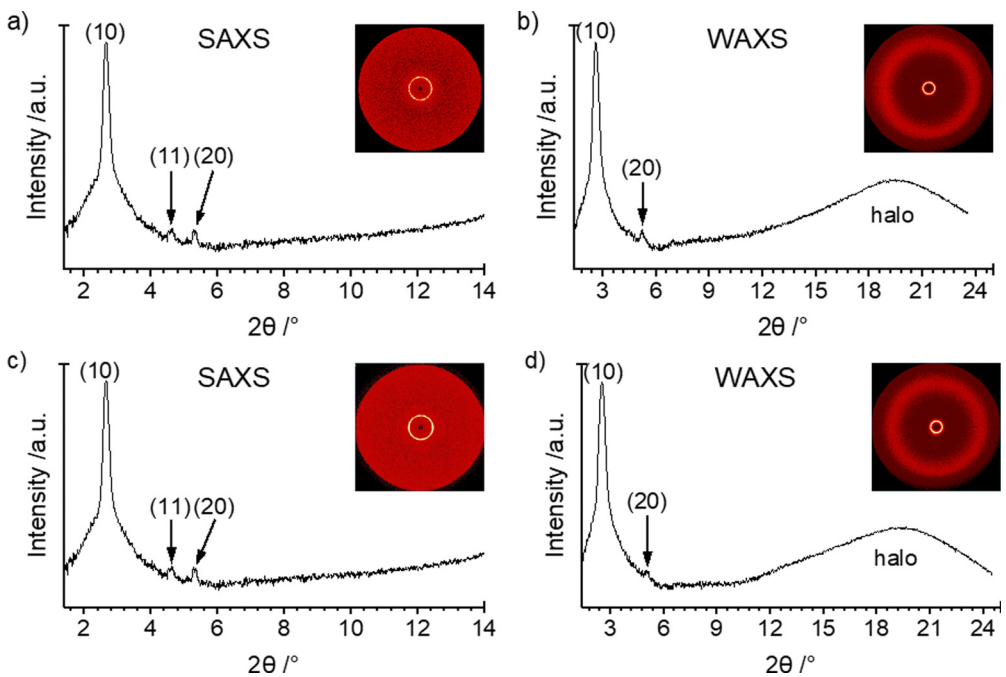

Fig. 5 (a) Small angle scattering (SAXS) and (b) wide angle scattering (WAXS) profile of **Gua(14)Br** at 65 °C upon cooling with the corresponding diffraction patterns (inset). (c) SAXS and (d) WAXS profiles of **Gua(14)PF$_6$** at 65 °C upon cooling with the corresponding diffraction patterns (inset).

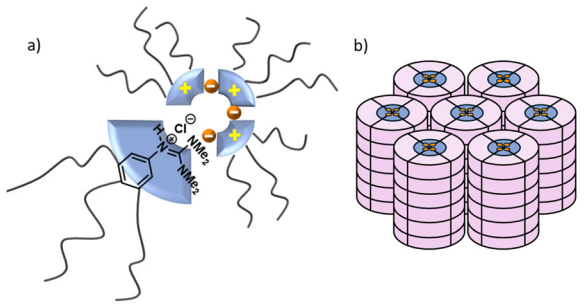

Fig. 6 (a) Possible packing model for the wedge-shaped guanidinium ILCs **Gua(14)X** with schematic representations in pizza slice-like form and (b) the hexagonal columnar (Col_h) mesophase: cationic head group (blue); anion (orange); periphery with chains (purple).

The thermal stabilities of the mesomorphic compounds were determined through TGA measurements. The detailed results can be found in Fig. S14 and Table S9 (ESI†). Overall, the compounds showed decomposition temperatures between 240 °C (**Gua(14)NO$_3$**) and 305 °C (**Gua(14)N(CN)$_2$**). However, for most compounds, decomposition started around 280 °C, *i.e.* far above the clearing temperatures.

Electrochemical studies of guanidinium ILCs

The redox stability of the mesomorphic guanidinium salts **Gua(14)X** was investigated by cyclic voltammetry (CV). The electrochemical stability window ΔEW is defined as the potential window where no significant oxidative or reductive processes of the sample occur, and consequently no noteworthy current can be observed when applying the CV potential.[50,85] Therefore, ΔEW is described by eqn (1) with E_{an} and E_{cat} being the respective anodic and cathodic potential limits of each individual compound.[86,87]

$$\Delta EW = E_{an} - E_{cat} \quad (1)$$

One of the obstacles for measuring ΔEW for the guanidinium salts **Gua(14)X** was their low solubility in solvents that are commonly used in CV measurements. Consequently, several factors had to be considered for the actual measurements: (I) use of the same solvent for all compounds (better comparison), (II) a reasonable solvent stability window in the cell set-up, (III) solubility of the internal standard (ferrocene) and conducting salt in the solvent for the measurement of a solvent stability window. Based on these factors, only dichloromethane (DCM) was suitable as a solvent for the CV measurements. The combination of DCM and ferrocene as well as Bu_4NPF_6 as conducting salt showed a stability window in the aforementioned cell set-up between +1.2 and −2.0 V.

Overall, for most compounds **Gua(14)X,** the oxidation end of ΔEW was determined by the cation. All compounds showed a distinctive oxidation peak around +0.9 V, which can therefore be attributed to the cation effect as only the cation remains unchanged (Fig. 7). The peak itself was slightly shifted depending on the anion but always appeared around +0.9 V (Table 3). It

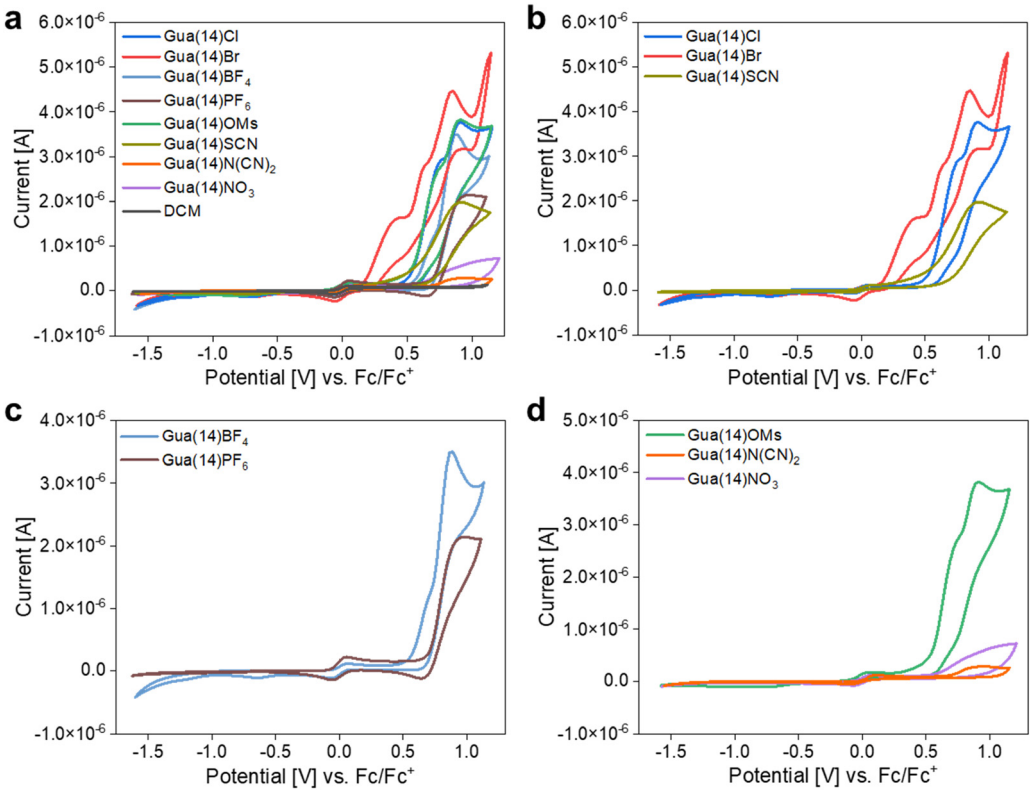

Fig. 7 (a) Cyclic voltammograms of all guanidinium salts **Gua(14)X**. Cyclic voltammograms of **Gua(14)** cations with (b) halide and pseudo-halide anions, (c) fluorine-containing anions, and (d) additional anions.

Table 3 Electrochemical properties of all guanidinium salts **Gua(14)X** studied

Compound	E_{an} [V *vs.* Fc/Fc$^+$] Peak maximum	Cut-off	E_{cat} [V *vs.* Fc/Fc$^+$]	ΔEW [V]$_{peak}$	ΔEW [V]$_{cut\text{-}off}$
Gua(14)Cl	0.91	0.47	−1.03	1.94	1.50
Gua(14)Br	0.45; 0.85	0.17	−1.10	1.95	1.27
Gua(14)I[b]	0.27; 0.61	0.08	[a]	[a]	[a]
Gua(14)BF4	0.87	0.55	−1.11	1.98	1.66
Gua(14)PF$_6$	0.97	0.66	−1.79	2.76	2.45
Gua(14)OMs	0.98	0.44	−1.82	2.80	2.26
Gua(14)SCN	0.96	0.31	−1.83	2.79	2.14
Gua(14)N(CN)$_2$[c]	0.96	0.79	−1.74	2.70	2.53 [c]
Gua(14)NO$_3$	[a]	0.66	−1.52	[a]	2.18

[a] Could not be determined. [b] Not referenced to Fc/Fc$^+$. [c] 1st CV cycle, as not reproducible in multiple cycles.

must be pointed out that a direct comparison with the literature data is not trivial as many of the guanidinium IL examples found in the literature are structurally only slightly similar to the guanidinium salts **Gua(14)X** investigated in this study. Most guanidinium derivatives for which CV data can be found in the literature are either part of a piperidinium structure or contain six alkyl chains of various lengths. The pure guanidinium trifluoromethane sulfonate investigated by Zhu *et al.* showed an anodic stability of at least +0.8 V (*vs.* pseudo Pt).[54] Several guanidinium ILs containing three different anions OTf, NTf_2, and $N(CN)_2$ studied by Gnahm *et al.*[55] exhibited maximum anodic potential limits of +0.6 V to +1.0 V when in contact with an Au surface and compared against. an Ag pseudo-reference electrode.

Similar compounds were also investigated by Berger *et al.*[56] Their guanidinium ILs showed anodic limits *vs.* Pt between +1 V and +1.4 V for different alkyl chain lengths and +1.5 V to +1.7 V for piperidinium-based ILs.[56] More guanidinium stability windows were described in the dissertation of Arkhipova,[63] ranging from +0.6 V to +1.6 V depending on the alkyl chains and anions, which were then further used in the investigation as possible electrolytes for lithium ion batteries in combination with lithium salts.[57,63] Other functionalized guanidinium ILs showed significantly higher anodic limits.[28,29,58] Aromatic complexes with guanidino-functionalized aromatic ligands which usually contain more than one guanidine-function also showed an oxidation process around +1 V.[59–62] An overview of the literature guanidinium compounds and their cyclic voltammetry data for better comparison can be found in Table S8 (ESI†).

Some of the guanidinium salts **Gua(14)X** (X = Cl, Br, OMs, SCN, I, BF_4) investigated in this study showed an influence of the anion upon the oxidation peak/cut-off potential or a limiting influence on the oxidative side of ΔEW, which will be discussed below. However, no such negative effect was observed for **Gua(14)N(CN)$_2$**, **Gua(14)NO$_3$** and **Gua(14)PF$_6$**, when analyzing the cut-off current (Table 3). Many of the anions represented in this study (BF_4, OMs and PF_6) have been used in previous electrochemical studies of ILs, showing that there are numerous instances of oxidative stability for substances containing these anions up to at least +2 V.[47,88–90] As a result, the peak around +1 V most likely originates in the cation. This observation is in agreement with a previous report by Himmel and co-workers,[62] indicating that guanidino-functionalized aromatic compounds can act as electron donors. Our hypothesis was also supported by DFT calculations (see below).

The guanidinium ILCs **Gua(14)X** containing halide anions displayed typical redox behavior associated with these halides. The most complex cyclic voltammogram was obtained for **Gua(14)I**. Multiple signals between +0.2 and +0.6 V (Fig. S12a, ESI†) could be attributed to the electrooxidation of the iodide anion, with the first oxidation peak corresponding to the oxidation of iodide to molecular iodine followed by the formation of the triiodide anion. The second oxidation peak was then assigned to the dissociation of said triiodide.[91–93]

The CV curves for the other guanidinium ILCs **Gua(14)X** with halide and pseudo halide counterions can be found in Fig. 7b. **Gua(14)Br** showed distinct peaks around +0.5 and +0.8 V with an additional shoulder at +0.7 V. These signals might be caused by the same mechanisms observed in **Gua(14)I** – namely the stepwise electrooxidation of the bromide anion.[94] Compared to the iodide anion, the potentials observed for bromide were shifted to higher values and the second oxidation steps might coincide with the oxidation of the cation; this could explain the prominent shoulder of the second peak. In contrast, the electrooxidation of the chloride anion was not visible in the CV data, as the potentials for the chloride oxidation steps seemed to be higher than for the oxidation of the guanidinium cation; this is consistent with the reports from the literature.[95]

Gua(14)SCN was another guanidinium salt for which an influence of the anion on the oxidation limit was observed. The oxidation peak was slightly shifted towards lower potentials and was also very broad. This behavior can be justified by the pseudo-halide nature of the SCN anion. This anion exhibits quasi-halide electrochemical behavior, forming an $(SCN)_2$ dimer upon oxidation.[48,96] This process might again overlap with the oxidation of the cation as seen for **Gua(14)Br**, resulting in a broad peak and a comparatively low cut-off potential.

No real peak was visible in the voltammogram of **Gua(14)NO$_3$** (Fig. 7d), as this compound only showed a broad oxidation signal. Even though this compound possessed one of the widest $\Delta EW_{cut\text{-}offs}$, the oxidation current measured in the three scans showed decreasing signal intensities with each scan (Fig. S12c, ESI†), indicating a depletion of ions and slow

diffusion close to and/or deactivation of the electrode surface by reaction products. Therefore, reproducible CV scans could not be obtained and no reliable statement on the oxidative stability of this compound could be made.

A similar observation was made for **Gua(14)N(CN)$_2$** (Fig. 7d). This compound showed one of the widest $\Delta EW_{cut\text{-}offs}$ and highest $E_{an,cut\text{-}off}$ for the 1st CV cycle. As ILs containing this anion were already shown to have oxidative stability up to +2 V, the oxidative process in this CV measurement might be attributed to the cation.[50,97] However, even in the 1st cycle, the experimental current was very low. Furthermore, the 2nd and 3rd cycles showed almost no current response when scanned in the same potential range. This non-reproducibility has already been observed for other guanidinium compounds containing the same anion.[55] These observations suggest that at least in part, the anion is also involved in the processes leading to the observed signals. Examples include, but are not limited to, the formation of the neutral dimer $(NC)_2N\text{–}N(CN)_2$.[97]

The most stable compounds towards reduction can be seen in Fig. 8. Here, **Gua(14)SCN**, **Gua(14)PF$_6$** and **Gua(14)OMs** showed the highest reductive stability. This high stability towards reduction has already been reported for compounds containing the OMs and PF_6 anion.[47,89,98–100]

When looking closely at the cyclic voltammograms of most compounds (except for **Gua(14)PF$_6$**, **Gua(14)N(CN)$_2$** and **Gua(14)NO$_3$**), a small broad reduction peak or deviation from the current baseline between −0.5 and −1.0 V was observed. This process seems to be more or less pronounced depending on the different guanidinium salts **Gua(14)X** (Fig. 7a). We suggest two possible causes for this observation, both of which are supported by the results of more detailed investigations: (I) presence of traces of water in the compounds, (II) delayed reduction of some oxidation products.

Fig. 9a and b show the voltammograms of DCM + ferrocene, as well as **Gua(14)OMs** with and without added water. Clearly, the presence of water influences the reduction side of the voltammogram between −0.5 and −1.0 V. There was no signal in the data obtained from pure DCM, and only a small signal was visible in the data obtained from pure **Gua(14)OMs**. The same signal increased upon the addition of water. This suggested that the process between −0.5 and −1.0 V detected for the different guanidinium salts **Gua(14)X** could be associated with the reduction of water. A limiting influence of water on the electrochemical stability window of ILs is well known.[50,89]

However, as already mentioned above, this additional signal could also be caused by the re-reduction of oxidation products. This can be illustrated as follows: Fig. 9c and d display comparisons of different measurements of **Gua(14)Br** and **Gua(14)Cl**. For **Gua(14)Br**, the comparison between measurements with and without ferrocene showed that in the measurement without ferrocene, which was (normalized to the measurement with ferrocene) only scanned to a potential of +0.8 V, no reduction peak was visible (Fig. 9c). The same result could be observed for **Gua(14)Cl**, where a sample without ferrocene was scanned to +0.8 V and +1.2 V (not referenced to Fc/Fc^+, Fig. 9d). The measurement up to +1.2 V showed a small peak at −0.4 V, whereas in the measurement stopped at a lower potential of +0.8 V, such a peak was absent, confirming the above hypothesis. However, as previously shown, the influence of traces of water could not be entirely ruled out. It is therefore not possible to exclusively assign this peak to either of the processes mentioned above, as they both are still reasonable possibilities at this stage.

In conclusion, the most significant limitation on ΔEW of the investigated compounds could be found for the anions, BF_4, Br, Cl, I, and SCN. In contrast, the highest $\Delta EW_{cut\text{-}off}$ that can reproducibly be measured was found for **Gua(14)PF$_6$** and the smallest $\Delta EW_{cut\text{-}off}$ was found for **Gua(14)Br** and **Gua(14)Cl** (Table 3).

Theoretical studies of guanidinium salts

It has been postulated above that for some guanidinium salts **Gua(14)X,** the distinctive peak at around +0.9 V (*vs.* Fc/Fc^+) originates in a cation oxidation process. To further support this hypothesis, DFT calculations were performed for **Gua(14)Br**, **Gua(14)NO$_3$** and **Gua(14)PF$_6$**. They were chosen as representative examples of compounds influenced by the anion (Br), seemingly not influenced by the anion (PF_6) and inconclusive

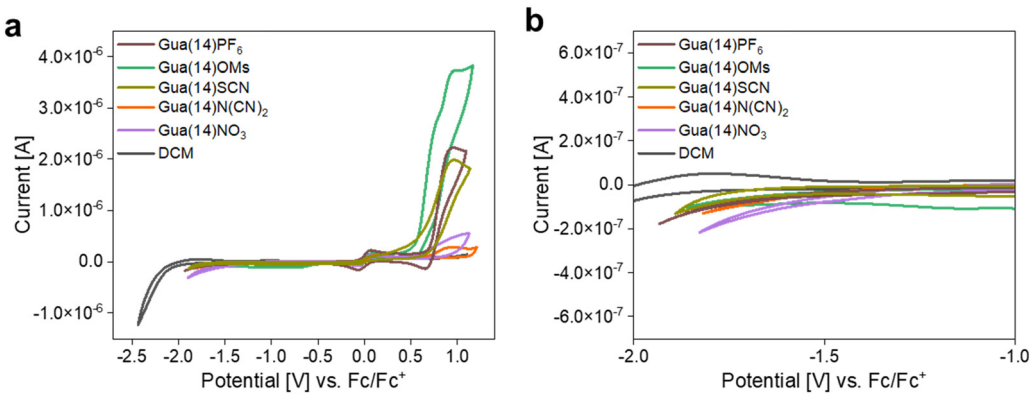

Fig. 8 (a) Cyclic voltammograms of selected guanidinium salts **Gua(14)X** scanned to lower potentials, (b) magnified view of cyclic voltammograms between −1.0 and −2.0 V.

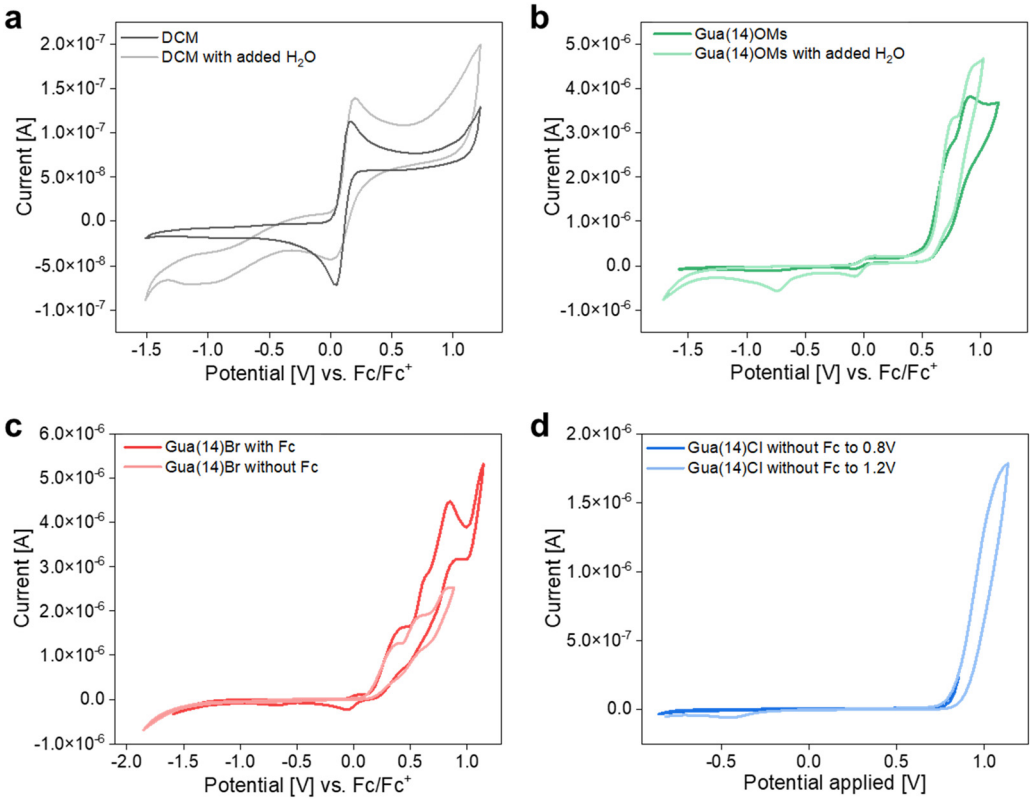

Fig. 9 (a) Cyclic voltammogram of DCM with and without water, (b) cyclic voltammogram of **Gua(14)OMs** with and without water, (c) cyclic voltammogram of **Gua(14)Br** with and without Fc and scanned to different potentials (curve without Fc normalized to the curve measured with Fc; original curves can be found in Fig. S12, ESI†), (d) cyclic voltammogram of **Gua(14)Cl** without Fc scanned to different end potentials.

with regard to the redox process (NO_3), when comparing ΔEW_{peak}. As CV measurements are based on redox processes and therefore electron transfers, an investigation of the HOMO (highest occupied molecular orbital) and LUMO (lowest unoccupied molecular orbital) energies for each anion in comparison to the respective cation energy is helpful for understanding the redox processes.[101,102]

All calculations were performed using the Gaussian 16 program package with the B3LYP, M062X, and PBE functionals and basis sets as implemented therein,[103] and carried out for isolated ions, *i.e.* a single anion or cation.

First test calculations were performed on guanidinium cations **Gua(n)** with different chain lengths *n* with B3LYP/6-31G* in order to investigate the influence of the alkyl chains on the HOMO and LUMO energies of the cation (Table S3, ESI†). The original cation **Gua(14)** and simplified versions with methyl **Gua(1)**, ethyl **Gua(2)**, propyl **Gua(3)** and butyl **Gua(4)** chains were tested. All structures were fully optimized starting from a "straight" chain conformation and the optimized structures for **Gua(2)** and **Gua(14)** are shown in Fig. S13 (ESI†). The calculations indicated that **Gua(2)** seems to be reasonably close to **Gua(14)**. Therefore, **Gua(2)** was used as a reference in the following investigations. Also **Gua(1)**, **Gua(3)** and **Gua(4)** were investigated to estimate the uncertainty introduced by the approximate treatment of the alkyl chains. **Gua(14)** was not used for further calculations because geometry optimization particularly when including polarizable continuum models (PCMs)[104] for dichloromethane (DCM) was difficult to converge for the long alkyl chains. Note that entropy effects or different conformations, which could lead to the different anodic limits for different alkyl chain lengths found in the experimental investigations reported above, are not considered here. In the following discussion, we only refer to **Gua(2)**. The full results can be found in the ESI† (Tables S4–S7).

As a next step, different basis sets, *i.e.* aug-cc-pVDZ and aug-cc-VTZ, were tested for the cations and the investigated anions, *i.e.* Br, NO_3 and PF_6, again using B3LYP with PCM for DCM and Grimme's D3 dispersion corrections.[105] These levels of theory are labeled as B3LYP/DZ and B3LYP/TZ in the following discussion. In order to test the influence of the used density functional, the same calculations were performed at the M062X-D3/aug-cc-pVDZ (label: M062X/DZ) and PBE-D3/aug-cc-pVDZ (label: PBE/DZ) level of theory. The respective ionization potentials relative to that of **Gua(2)** are given in eqn (2), *i.e.*,

$$IP_X^{HOMO} = -\varepsilon_{HOMO,X} + \varepsilon_{HOMO,Gua(2)} \quad (2)$$

where $\varepsilon_{HOMO,X}$ is the HOMO energy of the respective compound. The resulting values are given in Table 4 and Table S4 (ESI†). A negative value suggests that the compound would be oxidized more easily than **Gua(2)**, while a positive value suggests the opposite. The results depended only to a very small extent on the basis set or the length of the alkyl chain

(see Table S4, ESI†). However, the choice of the functional can lead to rather large differences up to 2 eV. We conclude from the IP_X^{HOMO} that only PF_6 has a higher IP than the cation, while the other anions have similar or slightly lower IPs.

Finally, ΔSCF calculations were performed to obtain vertical and relaxed ionization potentials. For this purpose, structures of the ions with one electron removed, *i.e.* the neutral form of the anions and doubly positively charged cations (ions-e^-) were optimized in addition to the structures of all anions and cations (ions). The following energy differences were calculated:

$$IP_X^{vert} = E_X^{ion\text{-}e^-}\left(R^{ion}\right) - E_X^{ion}\left(R^{ion}\right) \quad (3)$$

$$IP_X^{adia} = E_X^{ion\text{-}e^-}\left(R^{ion\text{-}e^-}\right) - E_X^{ion}\left(R^{ion}\right) \quad (4)$$

$$-EA_X^{vert} = E_X^{ion\text{-}e^-}\left(R^{ion\text{-}e^-}\right) - E_X^{ion}\left(R^{ion\text{-}e^-}\right) \quad (5)$$

where, for instance, $E_X^{ion\text{-}e^-}\left(R^{ion}\right)$ is the energy of the neutral form of the anions or doubly positively charged cations calculated at the respective optimized structures of the anions or the cations. $-EA_X^{vert}$ corresponds to the vertical ionization potential at the optimized structure of the ion-e^- species. The respective values are given in Table 4 and Table S7 (ESI†).

As observed, the Δ-SCF results for IP_X^{vert} showed similar trends to the HOMO-derived IPs. For IP_X^{adia}, all anions (except **Br** for M062X/DZ) possessed a larger IP than the cations.

This indicated that nuclear reorganization is much more important for the cation than for the anions. This assumption was also supported by the values of $-EA_X^{vert}$, which were again larger for the anions than for the cations (Table S7, ESI†). We expect that the IP_X^{vert} values are the ones which fit best to the experiment because of the probably rather long-time scale needed for the nuclear reorganization in the Gua(X) cations, *i.e.* we think that the electron transfer process is reasonably close to a vertical transition.

Overall, as already stated above, only the **PF_6** anion showed a higher IP_X^{vert} value than the cation, whereas **Br** and **NO_3** showed smaller IP_X^{vert} (Table 4). These results were in good agreement with the observations from the CV measurements (Fig. 6), as **Gua(14)Br** clearly showed oxidative processes that precede those of **Gua(14)PF_6**. However, **Gua(14)NO_3** did not show a distinct oxidation peak but rather a broad oxidation process. This might indicate an overlay between anion and cation processes. DFT calculations seem to support this interpretation because the results for IP_X^{vert} revealed that the value for the **NO_3** anion is very close to that of the guanidinium cation **Gua(2)**.

Table 4 IP_X^{HOMO}, *c.f.* eqn (2), derived from the HOMO energies of the optimized anions X, IP_X^{vert}, *c.f.* eqn (3), derived from Δ-SCF calculations, and IP_X^{adia}, *c.f.* eqn (4), derived from Δ-SCF calculations. All values are given in eV and relative to the IP of **Gua(2)**

		B3LYP/DZ	B3LYP/TZ	M062X/DZ	PBE/DZ
IP_X^{HOMO}	Br	−0.65	−0.64	−0.59	−0.75
	NO_3	−0.56	−0.55	0.12	−1.25
	PF_6	3.09	3.03	4.12	2.13
IP_X^{vert}	Br	−0.46	−0.50	−0.87	−0.25
	NO_3	−0.17	−0.18	−0.06	−0.45
	PF_6	3.43	3.37	4.08	2.65
IP_X^{adia}	Br	0.23	0.20	−0.10	0.36
	NO_3	0.46	0.45	0.63	0.11
	PF_6	4.09	4.03	3.56	3.25

Conclusion

To get some insight into counterion effects on the solution redox properties and bulk phase liquid crystalline self-assembly of ILCs, a series of wedge-shaped 3,4,5-(tris(tetradecyloxy))-phenylguanidinium salts **Gua(14)X** with different anions were prepared. Unfavorable acid–base equilibria of salts with counterions derived from weak acids precluded access to **Gua(14)X** with X = N_3, OAc, CN, OCN. In contrast, **Gua(14)X** with X = Cl, Br, I, BF_4, PF_6, $N(CN)_2$, SCN, NO_3, OMs could be isolated and characterized. These guanidinium ILCs formed stable enantiotropic Col_h mesophases. For ILCs with spherical anions (X = Cl, Br, I, BF_4, PF_6), clearing temperatures and mesophase ranges increased with the increasing size of the anion, except that BF_4 displayed the broadest phase and highest clearing transition. ILCs with non-spherical counterions seem to pack less efficiently in the Col_h phase, thus resulting in smaller phase widths and lower clearing transition. This trend is most obvious for the dicyanamide anion. In this particular case, the relatively large diameter of the anion and the less efficient packing in the mesophase resulted in the largest packing parameter *a*.

Electrochemical investigations of **Gua(14)X** revealed a distinctive oxidation around +0.9 V caused by the guanidinium cation. A contribution of the guanidinium cation to the oxidation signals was further supported by DFT calculations. The broadest electrochemical stability window was found for X = PF_6, while the smallest electrochemical stability window was found for X = Br. Overall, **Gua(14)PF_6** showed both the best electrochemical performance in solution, the highest mesophase stability (*i.e.* highest clearing temperature) and the broadest temperature range of the Col_h phase. Thus, this ILC seems to be the most promising candidate for further elaboration as an ordered electrolyte material. Future work must show whether this is indeed the case.

Author contributions

M. E. and E. W. synthesized and characterized the compounds and investigated the mesomorphic properties *via* POM and DSC. M. M. performed the XRD (WAXS, SAXS) studies. A. L. performed all electrochemical studies and wrote the electrochemical section of the manuscript. A. Z. wrote the manuscript and checked the data. T. K. performed the theoretical calculations and wrote the respective section. F. G. provided his expertise for the analysis of the XRD data. A. T. and S. L. coordinated and supervised the research and wrote the

manuscript. All coauthors proof-read the manuscript. M. E., A. L. and M. M. contributed equally to this work.

Conflicts of interest

There are no conflicts to declare.

Acknowledgements

Generous financial support by the Deutsche Forschungsgemeinschaft (LA 907/17-2, GI243/8-2, TA571/13-1, 13-2, 16-2 and HBFG and shared instrumentation grant no. INST 41/897-1 FUGG for 700 MHz-NMR), the Ministerium für Wissenschaft, Forschung und Kunst des Landes Baden-Württemberg, the Carl-Schneider Stiftung Aalen (shared instrumentation grant), the Bundesministerium für Bildung und Forschung (shared instrumentation grant # 01RI05177) is gratefully acknowledged.

References

1 N. Kapernaum, A. Lange, M. Ebert, M. A. Grunwald, C. Haege, S. Marino, A. Zens, A. Taubert, F. Giesselmann and S. Laschat, Current topics in ionic liquid crystals, *ChemPlusChem*, 2022, **87**, e202100397.
2 K. Goossens, K. Lava, C. W. Bielawski and K. Binnemans, Ionic liquid crystals: versatile materials, *Chem. Rev.*, 2016, **116**, 4643–4807.
3 M. Mansueto and S. Laschat, in *Handbook of Liquid Crystals*, ed. J. W. Goodby, C. Tschierske, H. F. Gleeson and P. Raynes, Wiley-VCH, Weinheim, 2nd edn, 2014, vol. 6, pp. 231–280.
4 K. V. Axenov and S. Laschat, Thermotropic Ionic Liquid Crystals, *Materials*, 2011, **4**, 206–259.
5 L. Douce, J.-M. Suisse, D. Guillon and A. Taubert, Imidazolium-based liquid crystals: a modular platform for versatile new materials with finely tuneable properties and behaviour, *Liq. Cryst.*, 2011, **38**, 1653–1661.
6 S. Chen and S. H. Eichhorn, Ionic Discotic Liquid Crystals, *Isr. J. Chem.*, 2012, **52**, 830–843.
7 V. Causin and G. Saielli, in *Green Solvents II: Properties and Applications of Ionic Liquids*, ed. A. Mohammad and D. Inamuddin, Springer, Dordrecht, 2012, pp. 79–118.
8 T. Kato and M. Yoshio, in *Electrochemical Aspects of Ionic Liquids*, ed. H. Ohno, John Wiley & Sons, Inc., Hoboken, NJ, USA, 2011, pp. 375–392.
9 K. Salikolimi, A. A. Sudhakar and Y. Ishida, Functional Ionic Liquid Crystals, *Langmuir*, 2020, **36**, 11702–11731.
10 T. Ichikawa, T. Kato and H. Ohno, Dimension control of ionic liquids, *Chem. Commun.*, 2019, **55**, 8205–8214.
11 X. Pan, M. Wang, X. Fang, C. Zhang, Z. Huo and S. Dai, Ionic liquid crystal-based electrolyte with enhanced charge transport for dye-sensitized solar cells, *Sci. China: Chem.*, 2013, **56**, 1463–1469.
12 W. S. Chi, H. Jeon, S. J. Kim, D. J. Kim and J. H. Kim, Ionic liquid crystals: Synthesis, structure and applications to I 2-free solid-state dye-sensitized solar cells, *Macromol. Res.*, 2013, **21**, 315–320.
13 N. Yamanaka, R. Kawano, W. Kubo, N. Masaki, T. Kitamura, Y. Wada, M. Watanabe and S. Yanagida, Dye-sensitized TiO2 solar cells using imidazolium-type ionic liquid crystal systems as effective electrolytes, *J. Phys. Chem. B*, 2007, **111**, 4763–4769.
14 N. Yamanaka, R. Kawano, W. Kubo, T. Kitamura, Y. Wada, M. Watanabe and S. Yanagida, Ionic liquid crystal as a hole transport layer of dye-sensitized solar cells, *Chem. Commun.*, 2005, 740–742.
15 R. Sasi, B. Chandrasekhar, N. Kalaiselvi and S. J. Devaki, Green Solid Ionic Liquid Crystalline Electrolyte Membranes with Anisotropic Channels for Efficient Li-Ion Batteries, *Adv. Sustainable Syst.*, 2017, **1**, 1600031.
16 T. Ito, S. Otobe, T. Oda, T. Kojima, S. Ono, M. Watanabe, Y. Kiyota, T. Misawa, S. Koguchi and M. Higuchi, Polymerizable ionic liquid crystals comprising polyoxometalate clusters toward inorganic-organic hybrid solid electrolytes, *Polymers*, 2017, **9**, 290.
17 R. Sasi, S. Sarojam and S. J. Devaki, High Performing Biobased Ionic Liquid Crystal Electrolytes for Supercapacitors, *ACS Sustainable Chem. Eng.*, 2016, **4**, 3535–3543.
18 M. Butschies, S. Sauer, E. Kessler, H. Siehl, B. Claasen, P. Fischer, W. Frey and S. Laschat, Influence of *N* -Alkyl Substituents and Counterions on the Structural and Mesomorphic Properties of Guanidinium Salts: Experiment and Quantum Chemical Calculations, *Chem. Phys. Chem.*, 2010, **11**, 3752–3765.
19 M. Butschies, M. Mansueto, J. C. Haenle, C. Schneck, S. Tussetschläger, F. Giesselmann and S. Laschat, Headgroups versus symmetry in congruent ion pairs: which one does the job in mesomorphic aryl guanidinium and aryl imidazolium sulphonates?, *Liq. Cryst.*, 2014, **41**, 821–838.
20 M. Butschies, M. Mansueto, J. C. Haenle, C. Schneck, S. Tussetschläger, F. Giesselmann and S. Laschat, Headgroups versus symmetry in congruent ion pairs: which one does the job in mesomorphic aryl guanidinium and aryl imidazolium sulphonates?, *Liq. Cryst.*, 2014, **41**, 821–838.
21 L. M. Antill, M. M. Neidhardt, J. Kirres, S. Beardsworth, M. Mansueto, A. Baro and S. Laschat, Ionic liquid crystals derived from guanidinium salts: induction of columnar mesophases by bending of the cationic core, *Liq. Cryst.*, 2014, **41**, 976–985.
22 S. Sauer, N. Steinke, A. Baro, S. Laschat, F. Giesselmann and W. Kantlehner, Guanidinium chlorides with triphenylene moieties displaying columnar mesophases, *Chem. Mater.*, 2008, **20**, 1909–1915.
23 M. Butschies, W. Frey and S. Laschat, Designer Ionic Liquid Crystals Based on Congruently Shaped Guanidinium Sulfonates, *Chem. – Eur. J.*, 2012, **18**, 3014–3022.
24 N. Trbojevic, J. C. Haenle, T. Wöhrle, J. Kirres and S. Laschat, Induction of ionic smectic C phases: a

systematic study of alkyl-linked guanidinium-based liquid crystals, *Liq. Cryst.*, 2016, **43**, 1135–1147.
25 N. Kapernaum, E. Wuckert, W. Frey, S. Marino, M. Wahl, F. Giesselmann and S. Laschat, Hunting for smectic C in calamitic azobenzene ionic liquid crystals with different cationic head groups, *J. Phys. Org. Chem.*, 2018, **31**, e3779.
26 E. Wuckert, M. D. Harjung, N. Kapernaum, C. Mueller, W. Frey, A. Baro, F. Giesselmann and S. Laschat, Photoresponsive ionic liquid crystals based on azobenzene guanidinium salts, *Phys. Chem. Chem. Phys.*, 2015, **17**, 8382–8392.
27 S. Fang, L. Yang, C. Wei, C. Jiang, K. Tachibana and K. Kamijima, Ionic liquids based on guanidinium cations and TFSI anion as potential electrolytes, *Electrochim. Acta*, 2009, **54**, 1752–1756.
28 S. Fang, L. Yang, J. Wang, H. Zhang, K. Tachibana and K. Kamijima, Guanidinium-based ionic liquids as new electrolytes for lithium battery, *J. Power Sources*, 2009, **191**, 619–622.
29 S. Fang, L. Yang, J. Wang, M. Li, K. Tachibana and K. Kamijima, Ionic liquids based on functionalized guanidinium cations and TFSI anion as potential electrolytes, *Electrochim. Acta*, 2009, **54**, 4269–4273.
30 D. S. Kim, A. Labouriau, M. D. Guiver and Y. S. Kim, Guanidinium-functionalized anion exchange polymer electrolytes via activated fluorophenyl-amine reaction, *Chem. Mater.*, 2011, **23**, 3795–3797.
31 J. Sarrato, A. L. Pinto, H. Cruz, N. Jordão, G. Malta, P. S. Branco, J. C. Lima and L. C. Branco, Effect of Iodide-Based Organic Salts and Ionic Liquid Additives in Dye-Sensitized Solar Cell Performance, *Nanomaterials*, 2022, **12**, 2988.
32 U. Wild, O. Hübner, M. Enders, E. Kaifer and H.-J. Himmel, Connecting Organic Redox-Active Building Blocks through Mild Noncatalytic C− H Activation, *Eur. J. Org. Chem.*, 2022, e202200349.
33 S. Haaf, E. Kaifer, H. Wadepohl and H.-J. Himmel, Use of Crown Ether Functions as Secondary Coordination Spheres for the Manipulation of Ligand–Metal Intramolecular Electron Transfer in Copper–Guanidine Complexes, *Chem. – Eur. J.*, 2021, **27**, 959–970.
34 L. Lohmeyer, E. Kaifer, H. Wadepohl and H.-J. Himmel, 1, 2, 5, 6-Tetrakis (guanidino)-Naphthalenes: Electron Donors, Fluorescent Probes and Redox-Active Ligands, *Chem. – Eur. J.*, 2020, **26**, 5834–5845.
35 C. Wagner, F. Kreis, D. Popp, O. Huebner, E. Kaifer and H.-J. Himmel, 1, 2, 4, 5-Tetrakis (tetramethylguanidino)-3, 6-diethynyl-benzenes: Fluorescent Probes, Redox-Active Ligands and Strong Organic Electron Donors, *Chem. – Eur. J.*, 2020, **26**, 10336–10347.
36 K. Mishiro, F. Hu, D. W. Paley, W. Min and T. H. Lambert, Macrosteres: the deltic guanidinium ion, *Eur. J. Org. Chem.*, 2016, 1655–1659.
37 J. S. Bandar and T. H. Lambert, Aminocyclopropenium ions: synthesis, properties, and applications, *Synthesis*, 2013, 2485–2498.
38 W. Ji, H. Huang, X. Zhang, D. Zheng, T. Ding, T. H. Lambert and D. Qu, A redox-active organic salt for safer Na-ion batteries, *Nano Energy*, 2020, **72**, 104705.
39 Z. M. Strater, M. Rauch, S. Jockusch and T. H. Lambert, Oxidizable Ketones: Persistent Radical Cations from the Single-Electron Oxidation of 2, 3-Diaminocyclopropenones, *Angew. Chem., Int. Ed.*, 2019, **58**, 8049–8052.
40 Y. Jiang, J. L. Freyer, P. Cotanda, S. D. Brucks, K. L. Killops, J. S. Bandar, C. Torsitano, N. P. Balsara, T. H. Lambert and L. M. Campos, The evolution of cyclopropenium ions into functional polyelectrolytes, *Nat. Commun.*, 2015, **6**, 5950.
41 P. J. Griffin, J. L. Freyer, N. Han, N. Geller, X. Yin, C. D. Gheewala, T. H. Lambert, L. M. Campos and K. I. Winey, Ion transport in cyclopropenium-based polymerized ionic liquids, *Macromolecules*, 2018, **51**, 1681–1687.
42 H. Huang, Z. M. Strater, M. Rauch, J. Shee, T. J. Sisto, C. Nuckolls and T. H. Lambert, Electrophotocatalysis with a trisaminocyclopropenium radical dication, *Angew. Chem., Int. Ed.*, 2019, **58**, 13318–13322.
43 B. Soberats, M. Yoshio, T. Ichikawa, H. Ohno and T. Kato, Zwitterionic liquid crystals as 1D and 3D lithium ion transport media, *J. Mater. Chem. A*, 2015, **3**, 11232–11238.
44 J. Sakuda, M. Yoshio, T. Ichikawa, H. Ohno and T. Kato, 2D assemblies of ionic liquid crystals based on imidazolium moieties: formation of ion-conductive layers, *New J. Chem.*, 2015, **39**, 4471–4477.
45 S. Wang, X. Liu, A. Wang, Z. Wang, J. Chen, Q. Zeng, X. Wang and L. Zhang, An ionic liquid crystal-based solid polymer electrolyte with desirable ion-conducting channels for superior performance ambient-temperature lithium batteries, *Polym. Chem.*, 2018, **9**, 4674–4682.
46 N. V. Shvedene, D. V. Chernyshov and I. V. Pletnev, Ionic liquids in electrochemical sensors, *Russ. J. Gen. Chem.*, 2008, **78**, 2507–2520.
47 J. Golding, S. Forsyth, D. R. Macfarlane, M. Forsyth and G. B. Deacon, Methanesulfonate and p-toluenesulfonate salts of the N-methyl-N-alkylpyrrolidinium and quaternary ammonium cations: novel low cost ionic liquids, *Green Chem.*, 2002, **4**, 223–229.
48 J. M. Pringle, J. Golding, C. M. Forsyth, G. B. Deacon, M. Forsyth and D. R. MacFarlane, Physical trends and structural features in organic salts of the thiocyanate anion, *J. Mater. Chem.*, 2002, **12**, 3475–3480.
49 W. Dobbs, L. Douce, L. Allouche, A. Louati, F. Malbosc and R. Welter, New ionic liquid crystals based on imidazolium salts, *New J. Chem.*, 2006, **30**, 528–532.
50 M. Hayyan, F. S. Mjalli, M. A. Hashim, I. M. AlNashef and T. X. Mei, Investigating the electrochemical windows of ionic liquids, *J. Ind. Eng. Chem.*, 2013, **19**, 106–112.
51 G. A. Tiago, I. A. Matias, A. P. Ribeiro and L. M. Martins, Application of ionic liquids in electrochemistry—Recent advances, *Molecules*, 2020, **25**, 5812.
52 S. T. Nestor, B. Heinrich, R. A. Sykora, X. Zhang, G. J. McManus, L. Douce and A. Mirjafari, Methimazolium-based ionic liquid crystals: Emergence of mesomorphic

properties via a sulfur motif, *Tetrahedron*, 2017, **73**, 5456–5460.

53 L. Veltri, G. Cavallo, A. Beneduci, P. Metrangolo, G. A. Corrente, M. Ursini, R. Romeo, G. Terraneo and B. Gabriele, Synthesis and thermotropic properties of new green electrochromic ionic liquid crystals, *New J. Chem.*, 2019, **43**, 18285–18293.

54 H. Zhu, U. Ali Rana, V. Ranganathan, L. Jin, L. A. O'Dell, D. R. MacFarlane and M. Forsyth, Proton transport behaviour and molecular dynamics in the guanidinium triflate solid and its mixtures with triflic acid, *J. Mater. Chem. A*, 2014, **2**, 681–691.

55 M. Gnahm, C. Berger, M. Arkhipova, H. Kunkel, T. Pajkossy, G. Maas and D. M. Kolb, The interfaces of Au (111) and Au (100) in a hexaalkyl-substituted guanidinium ionic liquid: an electrochemical and in situ STM study, *Phys. Chem. Chem. Phys.*, 2012, **14**, 10647–10652.

56 C. A. Berger, M. Arkhipova, G. Maas and T. Jacob, Dysprosium electrodeposition from a hexaalkylguanidinium-based ionic liquid, *Nanoscale*, 2016, **8**, 13997–14003.

57 S. Hess, M. Arkhipova, M. Wohlfahrt-Mehrens, G. Maas and M. Wachtler, Synthesis and characterization of guanidinium-based ionic liquids as possible electrolytes in lithium-ion batteries, *J. Electrochem. Soc.*, 2014, **161**, A753.

58 N. Bucher, S. Hartung, M. Arkhipova, D. Yu, P. Kratzer, G. Maas, M. Srinivasan and H. E. Hoster, A novel ionic liquid for Li ion batteries–uniting the advantages of guanidinium and piperidinium cations, *RSC Adv.*, 2014, **4**, 1996–2003.

59 B. Eberle, M. Damjanović, M. Enders, S. Leingang, J. Pfisterer, C. Krämer, O. Hübner, E. Kaifer and H.-J. Himmel, Radical Monocationic Guanidino-Functionalized Aromatic Compounds (GFAs) as Bridging Ligands in Dinuclear Metal Acetate Complexes: Synthesis, Electronic Structure, and Magnetic Coupling, *Inorg. Chem.*, 2016, **55**, 1683–1696.

60 C. Trumm, O. Hübner, P. Walter, S. Leingang, U. Wild, E. Kaifer, B. Eberle and H.-J. Himmel, One-versus Two-Electron Oxidation of Complexed Guanidino-Functionalized Aromatic Compounds, *Eur. J. Inorg. Chem.*, 2014, 6039–6050.

61 A. Peters, H. Herrmann, M. Magg, E. Kaifer and H.-J. Himmel, Tuning the Properties of Redox-Active Guanidino-Functionalized Aromatic Ligands by Substitution: Experiment and Theory, *Eur. J. Inorg. Chem.*, 2012, 1620–1631.

62 S. Stang, A. Lebkücher, P. Walter, E. Kaifer and H.-J. Himmel, Redox-Active Guanidine Ligands with Pyridine and p-Benzoquinone Backbones, *Eur. J. Inorg. Chem.*, 2012, 4833–4845.

63 M. Arkhipova, *Hexaalkylguanidinium Salts as Ionic Liquids – New Applications in Titanium and Aluminium Hexaalkylguanidinium Alcoholates Assisted Synthesis and as Electrolytes for Electrodeposition of Metals*, PhD thesis, University of Ulm, Institute of Organic Chemistry I, 2014.

64 M. Ebert, I. Carrasco, N. Dumait, W. Frey, A. Baro, A. Zens, M. Lehmann, G. Taupier, S. Cordier and E. Jacques, Joint venture of metal cluster and amphiphilic cationic minidendron resulting in near infrared emissive lamellar ionic liquid crystals, *Chem. – Eur. J.*, 2022, **28**, e202103446.

65 For selected examples see ref. 50–56.

66 I. Dumitru, F. L. Chiriac, M. Ilis, I. Pasuk, D. Manaila-Maximean, M. Micutz, T. Staicu and V. Cîrcu, Evidence of Counterion Size Effect on the Stability of Columnar Phase of Ionic Liquid Crystals Based on Pyridinium Salts Derived from N-3, 4, 5-Tri (alkyloxy)-benzyl-4-pyridones, *Crystals*, 2022, **12**, 715.

67 H. Bartsch, M. Bier and S. Dietrich, The role of counterions in ionic liquid crystals, *J. Chem. Phys.*, 2021, **154**, 014901.

68 L. Jacob, E. Rzeszotarska, M. Koyioni, R. Jakubowski, D. Pociecha, A. Pietrzak and P. Kaszynski, Tunable Intermolecular Charge Transfer in Ionic Liquid Crystalline Derivatives of the [closo-B10H10] 2–Anion, *Chem. Mater.*, 2022, **34**, 6476–6491.

69 N. del Giudice, M. L'Her, E. Scrafton, Y. Atoini, G. Gentile, B. Heinrich, R. Berthiot, A. Aliprandi and L. Douce, Luminescent Ionic Liquid Crystals Based on Naphthalene-Imidazolium Unit, *Eur. J. Org. Chem.*, 2021, 2091–2098.

70 J. Dai, K.-Q. Zhao, B.-Q. Wang, P. Hu, B. Heinrich and B. Donnio, Liquid crystal ionic self-assembly and anion-selective photoluminescence in discotic azatriphenylenes, *J. Mater. Chem. C*, 2020, **8**, 4215–4225.

71 M. Biswas, M. Dule, P. N. Samanta, S. Ghosh and T. K. Mandal, Imidazolium-based ionic liquids with different fatty acid anions: phase behavior, electronic structure and ionic conductivity investigation, *Phys. Chem. Chem. Phys.*, 2014, **16**, 16255–16263.

72 N. M. Mateus, L. C. Branco, N. M. Lourenço and C. A. Afonso, Synthesis and properties of tetra-alkyl-dimethylguanidinium salts as a potential new generation of ionic liquids, *Green Chem.*, 2003, **5**, 347–352.

73 P. S. Kulkarni, L. C. Branco, J. G. Crespo, M. C. Nunes, A. Raymundo and C. A. Afonso, Comparison of physicochemical properties of new ionic liquids based on imidazolium, quaternary ammonium, and guanidinium cations, *Chem. – Eur. J.*, 2007, **13**, 8478–8488.

74 P. Wang, S. M. Zakeeruddin, M. Grätzel, W. Kantlehner, J. Mezger, E. V. Stoyanov and O. Scherr, Novel room temperature ionic liquids of hexaalkyl substituted guanidinium salts for dye-sensitized solar cells, *Appl. Phys. A: Mater. Sci. Process.*, 2004, **79**, 73–77.

75 M. A. Grunwald, S. E. Hagenlocher, L. Turkanovic, S. M. Bauch, S. B. Wachsmann, L. A. Altevogt, M. Ebert, J. A. Knöller, A. R. Raab and F. Schulz, Does thermotropic liquid crystalline self-assembly control biological activity in amphiphilic amino acids? –tyrosine ILCs as a case study, *Phys. Chem. Chem. Phys.*, 2023, **25**, 17639–17656.

76 D. Lengvinaite, V. Klimavicius, V. Balevicius and K. Aidas, Computational NMR Study of Ion Pairing of 1-Decyl-3-methyl-imidazolium Chloride in Molecular Solvents, *J. Phys. Chem. B*, 2020, **124**, 10776–10786.

77 V. P. Swamy, H. V. Thulasiram, F. Rastrelli and G. Saielli, Ion pairing in 1-butyl-3-methylpyridinium halide ionic liquids studied using NMR and DFT calculations, *Phys. Chem. Chem. Phys.*, 2018, **20**, 11470–11480.

78 G. Saielli, Ion-pairing of octyl viologen diiodide in low-polar solvents: an experimental and computational study, *J. Phys. Chem. A*, 2008, **112**, 7987–7995.

79 A. G. Avent, P. A. Chaloner, M. P. Day, K. R. Seddon and T. Welton, Evidence for hydrogen bonding in solutions of 1-ethyl-3-methylimidazolium halides, and its implications for room-temperature halogenoaluminate (III) ionic liquids, *J. Chem. Soc., Dalton Trans.*, 1994, 3405–3413.

80 A. N. Pankratov and S. S. Khmelev, Acidity of HOCN, HSCN, HNCO, HNCS: A treatment from the viewpoint of ab initio approach, *J. Serbian Chem. Soc.*, 2005, **70**, 1183–1192.

81 J. Knelles, S. Beardsworth, K. Bader, J. R. Bruckner, A. Buehlmeyer, R. Forschner, K. Schweizer, W. Frey, F. Giesselmann and Y. Molard, Self-Assembly and Fluorescence of Tetracationic Liquid Crystalline Tetraphenylethene, *ChemPhysChem*, 2019, **20**, 2210–2216.

82 T. Kato, T. Yasuda, Y. Kamikawa and M. Yoshio, Self-assembly of functional columnar liquid crystals, *Chem. Commun.*, 2009, 729–739.

83 M. Butschies, J. C. Haenle, S. Tussetschlaeger and S. Laschat, Liquid crystalline guanidinium phenylalkoxybenzoates: towards room temperature liquid crystals via bending of the mesogenic core and the use of triflate counter ions, *Liq. Cryst.*, 2013, **40**, 52–71.

84 Y. Marcus, Thermodynamics of solvation of ions. Part 6.—The standard partial molar volumes of aqueous ions at 298.15 K, *J. Chem. Soc., Faraday Trans.*, 1993, **89**, 713–718.

85 A. Bhide, J. Hofmann, A. K. Dürr, J. Janek and P. Adelhelm, Electrochemical stability of non-aqueous electrolytes for sodium-ion batteries and their compatibility with Na 0.7 CoO 2, *Phys. Chem. Chem. Phys.*, 2014, **16**, 1987–1998.

86 N. De Vos, C. Maton and C. V. Stevens, Electrochemical stability of ionic liquids: general influences and degradation mechanisms, *ChemElectroChem*, 2014, **1**, 1258–1270.

87 S. Kazemiabnavi, Z. Zhang, K. Thornton and S. Banerjee, Electrochemical stability window of imidazolium-based ionic liquids as electrolytes for lithium batteries, *J. Phys. Chem. B*, 2016, **120**, 5691–5702.

88 A. Noda and M. Watanabe, Highly conductive polymer electrolytes prepared by in situ polymerization of vinyl monomers in room temperature molten salts, *Electrochim. Acta*, 2000, **45**, 1265–1270.

89 A. M. O'Mahony, D. S. Silvester, L. Aldous, C. Hardacre and R. G. Compton, Effect of water on the electrochemical window and potential limits of room-temperature ionic liquids, *J. Chem. Eng. Data*, 2008, **53**, 2884–2891.

90 J. Zhang and A. M. Bond, Practical considerations associated with voltammetric studies in room temperature ionic liquids, *Analyst*, 2005, **130**, 1132–1147.

91 E. I. Rogers, D. S. Silvester, L. Aldous, C. Hardacre and R. G. Compton, Electrooxidation of the iodides [C4mim] I, LiI, NaI, KI, RbI, and CsI in the room temperature ionic liquid [C4mim][NTf2], *J. Phys. Chem. C*, 2008, **112**, 6551–6557.

92 C. L. Bentley, A. M. Bond, A. F. Hollenkamp, P. J. Mahon and J. Zhang, Electrode reaction and mass-transport mechanisms associated with the iodide/triiodide couple in the ionic liquid 1-ethyl-3-methylimidazolium bis (trifluoromethanesulfonyl) imide, *J. Phys. Chem. C*, 2014, **118**, 22439–22449.

93 A. Ejigu, K. R. Lovelock, P. Licence and D. A. Walsh, Iodide/triiodide electrochemistry in ionic liquids: Effect of viscosity on mass transport, voltammetry and scanning electrochemical microscopy, *Electrochim. Acta*, 2011, **56**, 10313–10320.

94 G. D. Allen, M. C. Buzzeo, C. Villagrán, C. Hardacre and R. G. Compton, A mechanistic study of the electrooxidation of bromide in acetonitrile and the room temperature ionic liquid, 1-butyl-3-methylimidazolium bis (trifluoromethylsulfonyl) imide at platinum electrodes, *J. Electroanal. Chem.*, 2005, **575**, 311–320.

95 R. G. Compton and C. E. Banks, *Understanding voltammetry*, World Scientific, 2018.

96 M. Zistler, C. Schreiner, P. Wachter, P. Wasserscheid, D. Gerhard and H. J. Gores, Electrochemical characterization of 1-ethyl-3-methylimidazolium thiocyanate and measurement of triiodide diffusion coefficients in blends of two ionic liquids, *Int. J. Electrochem. Sci.*, 2008, **3**, 236–245.

97 D. R. Macfarlane, S. A. Forsyth, J. Golding and G. B. Deacon, Ionic liquids based on imidazolium, ammonium and pyrrolidinium salts of the dicyanamide anion, *Green Chem.*, 2002, **4**, 444–448.

98 J. L. Lebga-Nebane, S. E. Rock, J. Franclemont, D. Roy and S. Krishnan, Thermophysical properties and proton transport mechanisms of trialkylammonium and 1-alkyl-1 H-imidazol-3-ium protic ionic liquids, *Ind. Eng. Chem. Res.*, 2012, **51**, 14084–14098.

99 U. Schröder, J. D. Wadhawan, R. G. Compton, F. Marken, P. A. Suarez, C. S. Consorti, R. F. de Souza and J. Dupont, Water-induced accelerated ion diffusion: voltammetric studies in 1-methyl-3-[2, 6-(S)-dimethylocten-2-yl] imidazolium tetrafluoroborate, 1-butyl-3-methylimidazolium tetrafluoroborate and hexafluorophosphate ionic liquids, *New J. Chem.*, 2000, **24**, 1009–1015.

100 F. Zhao, X. Wu, M. Wang, Y. Liu, L. Gao and S. Dong, Electrochemical and bioelectrochemistry properties of room-temperature ionic liquids and carbon composite materials, *Anal. Chem.*, 2004, **76**, 4960–4967.

101 C. J. Margulis, H. V. Annapureddy, P. M. De Biase, D. Coker, J. Kohanoff and M. G. Del Pópolo, Dry excess electrons in room-temperature ionic liquids, *J. Am. Chem. Soc.*, 2011, **133**, 20186–20193.

102 N. R. Pitawela and S. K. Shaw, Imidazolium Triflate Ionic Liquids' Capacitance–Potential Relationships and Transport Properties Affected by Cation Chain Lengths, *ACS Meas. Sci. Au*, 2021, **1**, 117–130.

103 M. J. Frisch, G. W. Trucks, H. B. Schlegel, G. E. Scuseria, M. A. Robb, J. R. Cheeseman, G. Scalmani, V. Barone, G. A. Petersson, H. Nakatsuji, X. Li, M. Caricato, A. V. Marenich, J. Bloino, B. G. Janesko, R. Gomperts, B. Mennucci, H. P. Hratchian, J. V. Ortiz, A. F. Izmaylov, J. L. Sonnenberg, D. Williams-Young, F. Ding, F. Lipparini, F. Egidi, J. Goings, B. Peng, A. Petrone, T. Henderson, D. Ranasinghe, V. G. Zakrzewski, J. Gao, N. Rega, G. Zheng, W. Liang, M. Hada, M. Ehara, K. Toyota, R. Fukuda, J. Hasegawa, M. Ishida, T. Nakajima, Y. Honda, O. Kitao, H. Nakai, T. Vreven, K. Throssell, J. A. Montgomery Jr., J. E. Peralta, F. Ogliaro, M. J. Bearpark, J. J. Heyd, E. N. Brothers, K. N. Kudin, V. N. Staroverov, T. A. Keith, R. Kobayashi, J. Normand, K. Raghavachari, A. P. Rendell, J. C. Burant, S. S. Iyengar, J. Tomasi, M. Cossi, J. M. Millam, M. Klene, C. Adamo, R. Cammi, J. W. Ochterski, R. L. Martin, K. Morokuma, O. Farkas, J. B. Foresman and D. J. Fox, *Gaussian 16 Rev. C.01*, Wallingford, CT, 2016.

104 J. Tomasi, B. Mennucci and R. Cammi, Quantum mechanical continuum solvation models, *Chem. Rev.*, 2005, **105**, 2999–3094.

105 S. Grimme, J. Antony, S. Ehrlich and H. Krieg, A consistent and accurate ab initio parametrization of density functional dispersion correction (DFT-D) for the 94 elements H-Pu, *J. Chem. Phys.*, 2010, **132**, 154104.

